

Passes 10–18 (P010–P018), longitude of the wave 2 minimum -14°E ; 2. P037–P046, $+3^{\circ}\text{E}$; 3. P040–P049, $+3^{\circ}\text{E}$; 4. P045–P054, $+16^{\circ}\text{E}$; 5. P050–P059, $+15^{\circ}\text{E}$; 6. P055–P064, $+13^{\circ}\text{E}$; 7. P060–P069, -12°E ; 8. P065–P074, -3°E ; 9. P070–P079, -8°E ; 10. P068–P094, -18°E ; 11. P090–P099, -3°E ; 12. P095–P104, 1°E ; 13. P100–P109, -3°E ; 14. P105–P114, 8°E . The mean phase ± 1 standard deviation for the 14 cases is $2^{\circ}\text{E} \pm 10^{\circ}$ (for the wave 2 minimum). Variations in the time intervals of analysis is required to obtain

longitudinal coverage for changing orbital periods.
 24. G. Balmino, G. Moynot, N. Vales, *J. Geophys. Res.* **87**, 9735 (1982). D. E. Smith, and M. T. Zuber, *Science* **271**, 184 (1996).
 25. J. R. Barnes *et al.*, *J. Geophys. Res.* **101**, 12753 (1996). J. L. Hollingsworth and J. R. Barnes, *J. Atmos. Sci.* **53**, 428 (1996).
 26. J. B. Pollack *et al.*, *J. Geophys. Res.* **95**, 1447 (1990); J. R. Murphy *et al.*, *ibid.* **100**, 26357 (1995).
 27. A. I. F. Stewart, *LASP-JPL Internal Rep.*, PO# NQ-

802429, Jet Propulsion Laboratory, Pasadena, CA, March (1987).

28. R. T. Clancy and B. Sandor, private communication.
 29. We thank the Mars Surveyor Operations Project at Jet Propulsion Laboratory (JPL) and the MGS spacecraft operations team at Lockheed Martin Astronautics (Denver, CO) for their support in providing the MGS Accelerometer Team with the accelerometer and ancillary data used in this study. This work was funded in part by the JPL, Pasadena, CA.

20 January 1998; accepted 13 February 1998

Magnetic Field and Plasma Observations at Mars: Initial Results of the Mars Global Surveyor Mission

M. H. Acuña, J. E. P. Connerney, P. Wasilewski, R. P. Lin, K. A. Anderson, C. W. Carlson, J. McFadden, D. W. Curtis, D. Mitchell, H. Reme, C. Mazelle, J. A. Sauvaud, C. d'Uston, A. Cros, J. L. Medale, S. J. Bauer, P. Cloutier, M. Mayhew, D. Winterhalter, N. F. Ness

The magnetometer and electron reflectometer investigation (MAG/ER) on the Mars Global Surveyor spacecraft has obtained magnetic field and plasma observations throughout the near-Mars environment, from beyond the influence of Mars to just above the surface (at an altitude of ~ 100 kilometers). The solar wind interaction with Mars is in many ways similar to that at Venus and at an active comet, that is, primarily an ionospheric-atmospheric interaction. No significant planetary magnetic field of global scale has been detected to date ($< 2 \times 10^{21}$ Gauss-cubic centimeter), but here the discovery of multiple magnetic anomalies of small spatial scale in the crust of Mars is reported.

The Mars Global Surveyor (MGS) magnetic field experiment is identical to that developed for the Mars Observer Mission that failed to achieve Mars orbit in 1993 (1). The instrumentation provides fast vector measurements (up to 16 samples per second) of magnetic fields over a dynamic range of 0.005 to 65,536 nT per axis. The fundamental objectives of this investigation are to establish the nature of the magnetic field of Mars, to develop appropriate models

for its representation, and to map the crustal remnant field to a resolution consistent with spacecraft orbit altitude and ground track separation. The instrument complement includes two redundant triaxial fluxgate magnetometers and an electron reflectometer (1). The vector magnetometers provide in situ sensing of the ambient magnetic field in the vicinity of the MGS spacecraft over the automatically selected full-scale ranges of ± 4 nT to $\pm 65,536$ nT, with a digital resolution of 12 bits. The electron reflectometer measures the local electron distribution function in the range of ~ 1 eV to 20 KeV and will remotely sense the strength of the magnetic field down to the top of the martian atmosphere using directional information provided by the vector magnetometer. This synergistic combination was designed to increase the sensitivity and spatial resolution achievable from martian orbit with the vector magnetometer alone. Electron reflection magnetometry was first used on measurements from Apollo 15 and 16 Particles and Fields subsatellites (2).

Unlike Mars Observer, MGS lacks a boom to separate sensors from the spacecraft body to reduce interference by space-

craft-generated magnetic fields. Instead, each magnetometer sensor is placed at the outer edge of the articulated solar panels, about 5 m from the center of the spacecraft bus. The electron reflectometer sensor is mounted directly on the spacecraft nadir panel. This "twin magnetometer" configuration does not allow the real-time estimation of spacecraft fields (3) but provides redundancy and the near real-time detection and identification of spacecraft-generated magnetic fields. This instrument configuration required the design and implementation of magnetically "clean" solar array panels, which are used for aerobraking of the MGS spacecraft to achieve the final mapping orbit and are articulated about two orthogonal axes with respect to the spacecraft bus. Therefore, the orientation of the magnetic field sensors with respect to the spacecraft is variable and follows that of the solar panels, which are controlled to satisfy a variety of engineering requirements. The estimated accuracy of the measurements reported here is ± 0.5 nT before and after reconfiguration of the spacecraft for aerobraking, and ± 3 nT during the aerobraking phase. The magnetometer and electron reflectometer (MAG/ER) designs have extensive space flight heritage, and similar versions have been flown in numerous planetary and space physics missions. The instrument is operating nominally, and 2 to 16 vector samples per second of magnetic field data are acquired, depending on the telemetry rate supported by the telecommunication system.

The MGS spacecraft was inserted initially into a highly elliptical orbit with apoapsis > 10 Rm (1 Rm = Mars equatorial radius = 3397 km) and periapses as low as 112 km above the surface. The significant advantages of aerobraking orbits to the MAG/ER investigation were recognized early in the planning of the observations. In these orbits the spacecraft dips below the bottom of the martian ionosphere, allowing the MAG/ER experiment to achieve high sensitivity and spatial resolution for the detection of weak crustal fields. In addition, high plasma densities expected at these low altitudes required a different measurement technique, so a Langmuir probe operational

M. H. Acuña, J. E. P. Connerney, P. Wasilewski, NASA Goddard Space Flight Center, Greenbelt, MD 20771, USA.

R. P. Lin, Space Sciences Laboratory and Department of Physics, University of California, Berkeley, CA 94720, USA.

K. A. Anderson, C. W. Carlson, J. McFadden, D. W. Curtis, D. Mitchell, Space Sciences Laboratory, University of California, Berkeley, CA 94720, USA.

H. Reme, C. Mazelle, J. A. Sauvaud, C. d'Uston, A. Cros, J. L. Medale, Centre d'Etude Spatiale des Rayonnements, 31209 Toulouse Cedex, France.

S. J. Bauer, University of Graz and Space Research Institute, A-8010 Graz, Austria.

P. Cloutier, Department of Space Physics and Astronomy, Rice University, Houston, TX 77005, USA.

M. Mayhew, National Science Foundation, Arlington, VA 22230, USA.

D. Winterhalter, Jet Propulsion Laboratory, California Institute of Technology, Pasadena, CA 91109, USA.

N. F. Ness, Bartol Research Institute, University of Delaware, Newark, DE 19716, USA.

mode was added to the electron spectrometer, by using the outer case of the electrostatic analyzer as a swept bias collector.

We report here results obtained during the first 83 aerobraking orbits of MGS. The initial orbit plane was essentially normal to the Mars-sun direction, with a highly inclined line of apsides that placed the periapsis at 30° to 35°N latitude. As of orbit 83 (5 January 1997) the apoapsis radius has been reduced to 7.2 R_m, the orbit has precessed in local time to about the 2 a.m.–2 p.m. plane, and the latitude of periapsis has increased to 43°N with a typical altitude range of 108 to 120 km.

Solar wind interaction. As the spacecraft approaches the planet, it first encounters the bow shock at a distance of 2.33 R_m (12:33:24 UT) where the MAG/ER observes energized electrons, a sudden increase in magnetic field strength, and fluctuations associated with the shock crossing and martian magnetosheath (Fig. 1). The magnetic field on the day-side sheath region is turbulent, as determined by Phobos (4), the plasma is strongly energized, and the shock strength approaches the theoretical maximum. The behavior of the magnetic field as the spacecraft transits the ionosphere inbound and outbound implies that the solar wind is interacting directly with the martian ionosphere and neutral

atmosphere in a Venus-like interaction rather than in a magnetospheric interaction (5). The decrease in magnetic field magnitude within the ionosphere and the low-altitude magnetic field peak seen inbound (Fig. 1) just above the lower ionospheric boundary are typical characteristics of the Venus-solar wind interaction. The low field strength below the ionosphere (Fig. 1) rules out the possibility of a planet-wide magnetic field capable of providing a magnetospheric obstacle.

A mirror image signature, similar to the inbound leg, is observed on the outbound trajectory and bow shock crossing at 2.51 R_m (13:59:23 UT) (Fig. 1). At the beginning of the MGS aerobraking phase the spacecraft's orbital plane is oriented nearly parallel to the terminator plane, where the bow shock crossings are roughly symmetric inbound and outbound (Fig. 1). As the orbit precesses in local time, the inbound bow shock crossing is encountered tailward whereas the outbound crossing is encountered sunward of the dawn-dusk plane, giving rise to an asymmetry in the observed magnetic field and plasma profiles.

The locations of all well-defined bow shock crossings for the first 83 orbits reveal a shock surface that deviates from the average shape derived from previous Mars spacecraft observations (Fig. 2) (6). These

data represent an extensive set of observations of bow shock positions above and below the ecliptic plane of Mars. Several authors (7, 8) have noted the apparent independence of the martian bow shock position on upstream dynamic pressure. Because our data were obtained near solar minimum, one possible explanation is that the bow shock shape depends on solar extreme ultraviolet (EUV) flux (5). However, Slavin *et al.* (6) found no evidence for a solar cycle effect between mid-solar cycle (Mars 2, 3, and 5) and solar maximum (Phobos 2). Because we now know that the obstacle is the ionosphere and neutral atmosphere, another possibility is that the bow shock surface is asymmetric about the Mars-sun line because of obstacle asymmetries that have been theoretically predicted. Cloutier *et al.* (9) described two possible sources of asymmetry associated with planetary photo-ion pickup: one associated with the convection electric field, accelerating ions inward in one hemisphere and outward in the opposite hemisphere, and the other associated with the changing of the angle between the velocity and magnetic field vectors with magnetic latitude. The kinematics of newly ionized planetary exospheric neutral atoms (primarily O⁺) with large gyroradii could be important in defining the morphology of the Mars-solar wind interaction, and predicted asymmetries of O⁺ ions have been observed at Venus (10). Viscous effects of solar wind flow over the ionosphere can also produce asymmetric drag (11). A kinematic model by Brecht (12) produced an asymmetric shock flaring also aligned with the convection electric field, as might be expected from the O⁺ mass loading asymmetry. It is therefore expected that the bow shock position may respond to variations in the solar wind and interplanetary magnetic field orientation. The limited data set available to date precludes a definitive correlation of the bow

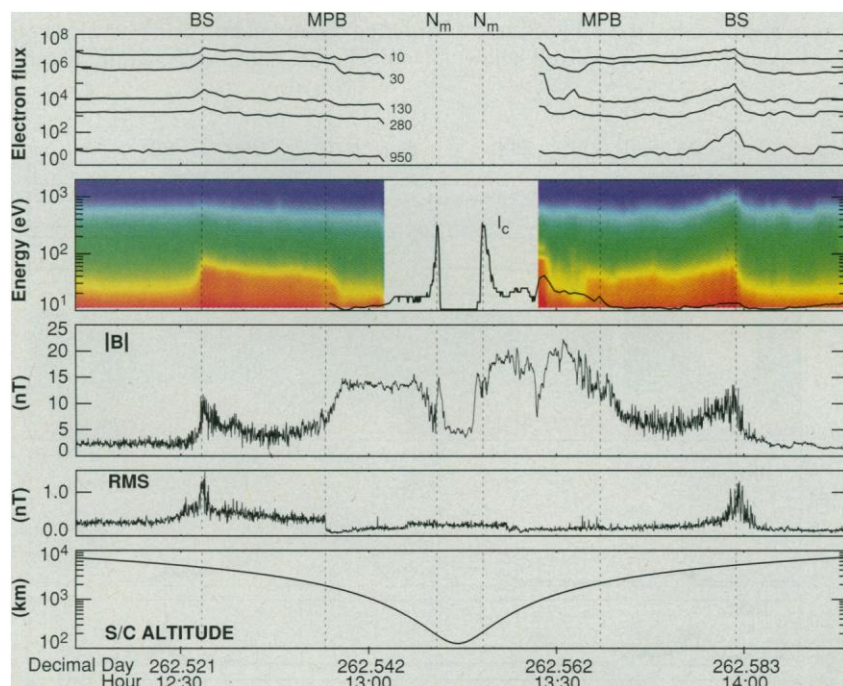


Fig. 1. Electron and magnetic field observations for day 262 (orbit 5). Electron fluxes (in units of $\text{cm}^{-2} \text{s}^{-1} \text{sr}^{-1} \text{eV}^{-1}$) are shown as line traces at five energies (10, 50, 130, 300, and 1000 eV; top to bottom, upper panel) and as a color spectrogram (second panel) with the relative density of cold (<10 eV) electrons superimposed by using the same number of logarithmic intervals as the spectrogram's energy scale. The next three panels show the magnetic field amplitude and root means square (RMS) and the spacecraft altitude. Vertical lines indicate the locations of the bow shock (BS), magnetic pile-up boundary (MPB), and ionospheric main peak (N_m).

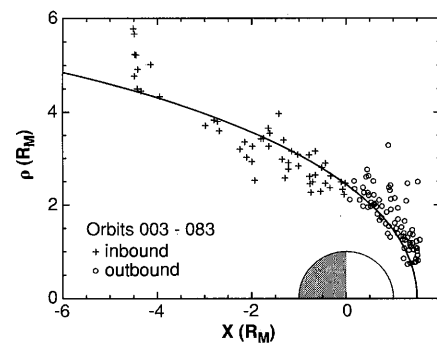


Fig. 2. Location of Mars bow shock crossings observed by MGS during the first 83 orbits. Distance (ρ) from the Mars-sun line (+x direction) is given for all bow shocks identified inbound (+) toward periapsis and outbound (*) from periapsis.

shock positions to IMF polarity and solar EUV flux.

The observed bow shock positions (Fig. 2) are variable, with a root-mean-square (rms) deviation about the average position near the terminator plane of about 0.5 Rm. Previous spacecraft observations at Mars show similar bow shock position variability, which is twice that observed at Venus (8). This variability could be associated with the presence of an intrinsic magnetic field strong enough to provide a degree of compressibility to the effective solar wind obstacle. If this was the case, then the shock position should depend on the strength and morphology of the intrinsic field in addition to solar wind parameters. However, all observations carried out to date from the aerobraking orbits do not provide evidence for a global magnetic field of sufficient strength to contribute significantly to the effective

size of the obstacle presented by Mars to the solar wind.

The draping of the interplanetary magnetic field around the ionospheric obstacle presented by Mars is clearly seen when the measured magnetic field vectors and the spacecraft trajectory corresponding to day 262 (orbit 5) are projected onto the Mars orbit plane (Fig. 3). Turbulent magnetic fields and energized electrons are observed throughout the magnetosheath region, between the bow shock and a characteristic boundary that we will refer to as the magnetic pile-up boundary (MPB) (Figs. 1, 3, and 4). As the spacecraft passes into this region the magnetic vector rotates, its mean amplitude begins to increase, fluctuations are reduced, and energetic electron fluxes begin to decrease. Some of the observed features of the ionospheric magnetic field are similar to those predicted by magneto-hydrodynamics models of the martian ionosphere (13). Observations of the solar wind interaction with the active comets Halley and Grigg-Skjellerup by the Giotto experiments (14) have shown evidence of the MPB, and similar magnetic field signatures were detected at Mars by the Phobos-2 MAGMA instrument (15). Ion measurements by the ASPERA and HARP (16) experiments aboard the same spacecraft also identified an ion composition boundary inside of which ions of planetary origin (that is, O⁺) dominate (7).

Periapsis altitudes for most MGS aerobraking orbits to date have been well below

150 km. At this altitude the ambient pressure is sufficiently high that the electron reflectometer's high voltage must be turned off to avoid electrical discharge or arcing in the instrument. During this portion of the orbit, the Langmuir probe collector of the ER continues to operate. The probe data must be interpreted with care because the instrument is mounted on the spacecraft body and at times the field of view encompasses the spacecraft's ion wake. The Langmuir probe data obtained during the first 15 orbits were unaffected by the spacecraft (Fig. 1). For orbits 20 through 36 the ER field of view was affected by ion wake effects at 210-km altitude inbound, which disappeared at 310 km outbound, preventing the measurement of the main ionospheric peak (Fig. 4). For orbits 19 through 36 periapsis was raised to 170 km, and for orbits 22 through 36 the ER main electrostatic analyzer could be operated continuously, allowing electron data to be obtained at these low altitudes, with energies between 1 eV and 20 KeV. At times cold (1 to <10 eV) and energetic (~>50 eV) electron fluxes were observed to be variable inside the MPB and often anticorrelated (Fig. 4). At altitudes between 300 and 500 km (solar zenith angle between 75° and 90°), the energetic electron flux drops abruptly by nearly an order of magnitude (Fig. 4). This altitude range corresponds to the location of the martian ionopause as inferred from radio occultation profiles (17). The ER does not generally observe a

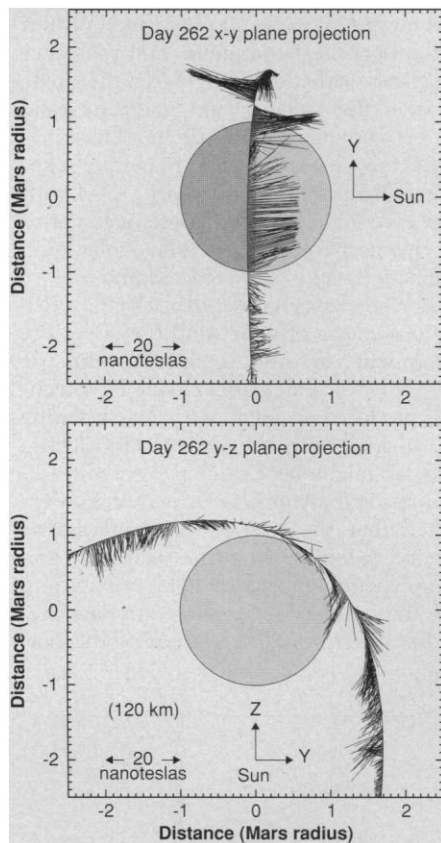


Fig. 3. (Top) Projection of the MGS spacecraft trajectory and observed magnetic field (**B**) vectors onto the Mars orbit plane for day 262 (orbit 5). The field observed along the trajectory at 12-s intervals is represented by a scaled vector projection of **B** originating from the position of the spacecraft at such times. Distance is given in units of Mars radius (3397 km), and field vectors are scaled to 20 nT = 1 Rm. (Bottom) Projection of the MGS spacecraft trajectory and observed magnetic field onto a plane perpendicular to the Mars orbit plane and the Mars-sun line. The spacecraft trajectory is nearly confined to this plane at this time.

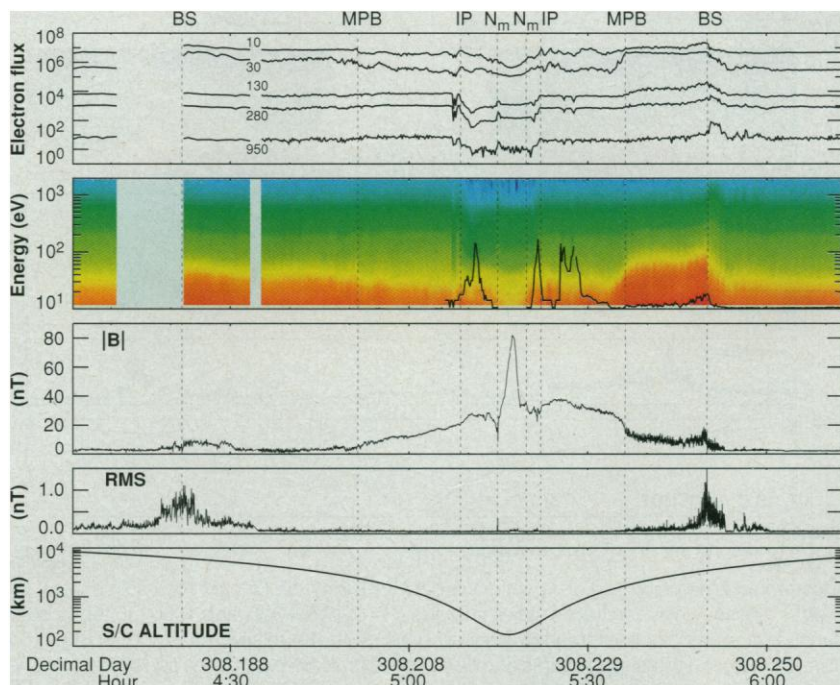


Fig. 4. Electron and magnetic field observations for day 308 (orbit 34). See caption to Fig. 1. Additional vertical lines indicate the location of the ionopause (P).

large gradient in the cold electron density at the ionopause, as defined by the abrupt drop in energetic electrons, and significant cold electron densities are often observed above the ionopause (Fig. 4). Impact ionization at Mars' night-side ionosphere was reported by Verigin *et al.* (18).

These cold electrons above the ionopause may indicate the presence of clouds or streamers of cold ionospheric plasma detaching from the ionopause, as was frequently observed at Venus (19). The innermost plasma boundary for orbits 4 to 15 occurs at an altitude of 180 to 210 km, where the cold electron density reaches a maximum (Fig. 1). This is likely the ionospheric main peak (a Chapman layer was observed at high solar zenith angles, 90° to 95°), although its altitude is somewhat higher than expected on the basis of radio occultation data (20). Just below this peak the contribution of atmospheric photoelectrons to the 10- to 50-eV electron flux drops, permitting a rough determination of the location of the ionospheric main peak when Langmuir probe measurements are unavailable (Fig. 4). Energetic electron fluxes do not decrease in the narrow altitude range sampled beneath the iono-

sphere main peak because the spacecraft is still above the atmospheric absorption heights for these energies (120 km at 2 keV). The energy distribution of these electrons is solar wind-like, implying the existence of an access mechanism, presently unexplained, between low altitudes and the solar wind at Mars.

Planetary magnetic field. Mars, like Venus, lacks an appreciable magnetic field of internal origin. The first observations of magnetic fields and plasmas in the near-Mars environment were obtained by the Mariner IV spacecraft as it passed within 13,200 km (3.89 R_M) of Mars in 1965. The lack of a detectable radiation belt (21) or magnetic field signature (22) attributable to Mars led to the conclusion that a martian magnetic moment could not exceed 10^{-3} that of Earth's dipole moment (8.0×10^{25} G-cm³). Subsequent observations were obtained by the Mars 2, 3, and 5 spacecraft in the early 1970s (21, 22) and the Mars Phobos-2 spacecraft in 1989 (4). These measurements, even those obtained by Phobos-2 to altitudes of 850 km of the surface of Mars, did not provide evidence of an intrinsic magnetic field. Several researchers suggested that there was a small intrinsic dipole moment of about 1×10^{22} to 2×10^{22} G-cm³ (23), whereas others said that no intrinsic field had been detected (4, 24). A magnetic moment of 1×10^{22} to 2×10^{22} G-cm³ would result in an equatorial surface field of 25 to 50 nT.

MGS is the first spacecraft to obtain magnetic field observations beneath the ionosphere (~170 to 200 km) in a region shielded from the confounding effects of the solar wind interaction with Mars, its atmosphere, and ionosphere. The magnetic fields associated with the MPB and the ionospheric obstacle presented to the solar wind can reach levels that could be confused with those arising from a planetary field of internal origin. Hence, the importance of obtaining measurements well below the bottom of the ionosphere cannot be overemphasized. The observations of day 262 (Figs. 1 and 3) illustrate one of many periapsis passes during which a relatively weak field (≤ 5 nT) was observed beneath the ionosphere. From this and similar periapsis passes at different longitudes we conclude that any present-day global-scale magnetic field cannot exceed an equatorial field strength of 5 nT. This represents an upper limit for a Mars dipole moment of $\sim 2 \times 10^{21}$ G-cm³, about a factor of 5 or 10 smaller than the most recent estimates derived from the Phobos results. The accuracy of the lower bound estimate for the magnetic moment is presently limited by our incomplete knowledge of the MGS spacecraft field in the aerobraking configuration. It is,

however, already clear that the immediate environment of Mars and its interaction with the solar wind is not significantly influenced by a global-scale, planetary magnetic field like that associated with all of the major planets in our solar system (25) except Venus and perhaps Pluto.

The lack of an appreciable present-day planetary magnetic field at Mars, coupled with the knowledge that Mars most likely had such a field in the past, suggests that its dynamo simply stopped working some time ago. This observation constrains the composition and thermal history of the Mars interior. Dynamo generation of a magnetic field in the interior of Mars requires the convective motion of an electrically conducting fluid interior, as well as a source of energy—for example, solidification of an inner core and resulting thermal convection—to power the dynamo. Models of the composition and thermal history (26) suggest several possibilities for the extinction of a once active Mars dynamo. A differentiated Mars interior is assumed to have an iron-rich core with a radius of about 1500 km (26). The presence of a lighter alloying element, sulfur, in the fluid core essentially determines if a solid iron inner core ever forms, or if so, how long the process takes. A core with more than about 15 weight % S does not form a solid inner core; one with substantially less forms a solid inner core that grows rapidly on a geologic time scale once it begins to freeze out. The less weight % S in the core, the earlier solid core formation begins. The lack of a present-day magnetic field suggests that the core has either largely frozen out (small initial weight % S) or never formed (large initial weight % S). If we can date the extinction of the dynamo by analysis of the distribution of magnetic anomalies in the Mars crust, we may be able to estimate the weight % S in the core as it initially formed.

Crustal magnetic anomalies. MGS aerobraking maneuvers have provided 83 periapsis passes with close-approach altitudes between 100 and 170 km. Most periapses have occurred at an altitude of about 110 km, between 32° and 35° N latitude, and are more or less randomly distributed in longitude. During many of these passes, the MAG experiment on MGS recorded large magnetic fields when the MGS spacecraft was beneath the ionosphere and close to the surface of Mars. The magnetic field profile observed during one such pass (day 264, orbit 6) shows a magnetic signature that is not of global scale; it is localized to a segment of the spacecraft trajectory that passes closely over the Mars crust (Fig. 5, top). Two isolated and distinct magnetic anomalies were actually observed along this trajectory, the largest near 32.9° N latitude, 22.4° W longitude, and

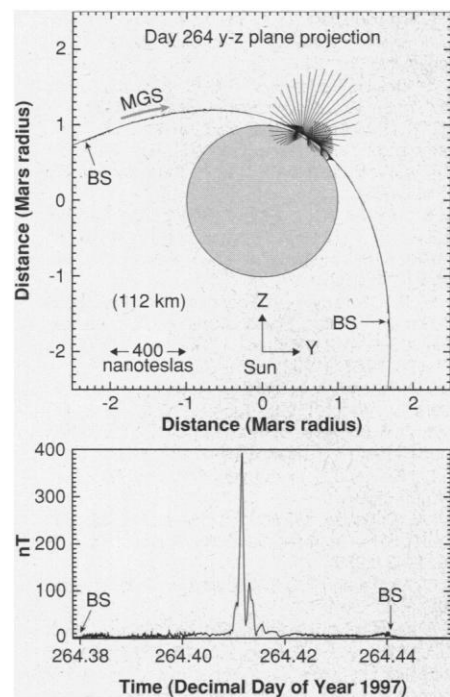


Fig. 5. (Top) Projection of the MGS spacecraft trajectory and observed magnetic field onto a plane perpendicular to the Mars orbit plane and the Mars-sun line for periapsis pass number 6 on day 264. The field observed along the trajectory at 3-s intervals is represented by a scaled vector projection of **B** originating from the position of the spacecraft at such times. Field vectors are scaled to 400 nT = 1 R_M. **(Bottom)** Magnitude of the observed magnetic field as a function of time for the interval of time represented in the top panel.

the smaller near 22.8°N latitude and 23.6°W longitude (Fig. 5).

The small spatial scale of these features can be appreciated by noting how far the spacecraft moves along the trajectory in the time spanned by the magnetic field signature. Quantitatively, the signature width is measured by joining the two points where the field strength is equal to half the maximum field measured [full width at half maximum (FWHM)]. The FWHM of the larger magnetic signature is about 50 s in duration, during which time the spacecraft moves ~218 km. A reasonable estimate of the distance to the source (upper limit) may be obtained without detailed knowledge of the source by assuming that it is produced by a vertically aligned dipole of finite extent located just beneath the spacecraft trajectory. The distance to the top of such a source is estimated to be ~200 km if the pole separation is small (<50 km) or ~150 km if the pole separation is large (>100 km) compared with the distance to the source. This translates to an estimated depth in the crust of between 40 and 90 km, allowing for the 112-km spacecraft altitude at the time of measurement. The presence of this pair of anomalies has been confirmed by a subsequent periapsis pass over essentially the same ground track but at a higher altitude. Nearby periapsis passes suggest that these features may be part of a larger system of east-west-trending linear anomalies.

Additional magnetic anomalies have been observed during other periapsis passes, all characterized by a FWHM roughly comparable to the spacecraft altitude at the time of observation. This suggests that the spatial extent of the sources is not significantly larger than the altitude of the spacecraft (~110 km at periapsis). Noting that the magnetic field of a dipole decreases as the cube of the distance from the source, it is clear that we can detect crustal anomalies within a band of planetary latitudes ($\pm 15^\circ$) centered on the latitude of periapsis (32° to 35°N thus far). For us to detect the same anomaly on a subsequent periapsis pass, the sub-spacecraft orbit track must pass within a few degrees in longitude of the anomaly (2° of longitude at the equator = 120 km) at periapsis.

A sufficiently dense and uniformly distributed sampling of the Mars crust is required for mapping purposes at spatial resolutions consistent with the MGS orbit altitude. To date the periapsis longitudes in the aerobraking orbits have been distributed more or less randomly as the latitude of periapsis drifts slowly northward, making the study of the spatial distribution of magnetic anomalies difficult. With this limited sampling of the Mars crust available this early in the mission, it is premature to discuss in detail the distribution of anomalies. However,

we note that anomalies with positive and negative radial moments have been detected, and that the largest anomalies (peak field magnitudes >100 nT) detected with the narrow band of latitudes sampled thus far (near 30°N) do not appear to be randomly distributed in longitude. These appear to be concentrated in the 120° longitude sector between 270° and 30°W longitude, roughly coincident with the most heavily cratered and oldest terrain at this latitude. This is contrary to some earlier proposals (27) that assumed that the largest magnetic anomalies would be found in association with relatively young volcanically emplaced material in the Tharsis region (90° to 150°W longitude).

A reasonably detailed map of crustal magnetic anomalies provides valuable clues regarding the early history of the Mars dynamo, crustal evolution, and composition. A possible origin of such anomalies involves an iron-rich magma (intrusive, impact, or thermal event) cooling in the presence of a primordial Mars magnetic field and acquiring a permanent remnant field that records the orientation of the global Mars magnetic field at that epoch. The extinction of the dynamo would then leave those anomalies that are not obliterated by subsequent thermal events as a permanent record of the paleofield and crustal evolution.

The magnitude of the magnetic field observed at satellite altitude implies a source in Mars' crust with a magnetic moment of $\sim 1.6 \times 10^{16}$ A-m² (1 A-m² = 10³ G-cm³). We estimate the source volume by taking a cube with sides of 100 km (the FWHM of the magnetic field signature implies that the source cannot be appreciably larger in spatial extent than the satellite altitude or ~118 km). To obtain the required moment, there must be a block of crustal material uniformly magnetized with a remnant magnetization of $\sim 5 \times 10^{-3}$ A-m²/kg. This value is ~500 times the magnetization of the SNC martian meteorites (28). The volume magnetization required (~ 16 A-m⁻¹) is comparable to that of strongly magnetic terrestrial crustal rocks associated with the most prominent crustal anomalies (29) measured by the MAGSAT spacecraft (Magnetic Satellite) mission of the late 1970s and early 1980s (30).

Finally, the complex magnetic field surface morphology of Mars raises the possibility that some of the observed bow shock position variability could be explained by the changing orientation of locally magnetized regions as the planet rotates (31).

REFERENCES AND NOTES

1. M. H. Acuña *et al.*, *J. Geophys. Res.* **97**, 7799 (1992).
2. K. A. Anderson *et al.*, *Proc. VI Lunar Sci. Conf.* **3**, 2971 (1975); R. P. Lin *et al.*, *Proc. VII Lunar Sci. Conf.*

- 3; 2691 (1976).
3. K. W. Behannon *et al.*, *Space Sci. Rev.* **21**, 235 (1977).
4. W. Riedler *et al.*, *Nature* **341**, 604 (1989).
5. A Venus-like interaction is defined as that associated with a planet that has no intrinsic magnetic field but a substantial atmosphere. Under these conditions the solar wind can reach directly to the top of the ionosphere. See, for example, T. K. Breus, in *Venus and Mars: Atmospheres, Ionospheres and Solar Wind Interactions* (Monograph 66, American Geophysical Union, Washington, DC, 1992), p. 387.
6. J. A. Slavin *et al.*, *J. Geophys. Res.* **96**, 11235 (1991).
7. T. K. Breus *et al.*, *ibid.*, p. 11165.
8. M. I. Verigin *et al.*, *ibid.* **98**, 1303 (1993).
9. P. A. Cloutier, R. E. Daniell, D. M. Butler, *Planet. Space Sci.* **22**, 967 (1974).
10. D. S. Intrilligator, *Geophys. Res. Lett.* **16**, 167 (1989).
11. H. Perez de Tejada, *J. Geophys. Res.* **96**, 11155 (1991); E. M. Dubinin *et al.*, *ibid.* **101**, 27061 (1996).
12. S. H. Brecht, *ibid.* **102**, 4743 (1997).
13. H. Shinagawa and T. Cravens, *ibid.* **94**, 6506 (1989); *ibid.* **97**, 1027 (1992).
14. C. Mazelle *et al.*, *Geophys. Res. Lett.* **16**, 1035 (1989); H. Reme *et al.*, *J. Geophys. Res.* **98**, 20965 (1993).
15. W. Riedler *et al.*, *Planet. Space Sci.* **39** (no. 1/2), 75 (1991).
16. N. M. Shutte *et al.*, *Nature* **341**, 614 (1989).
17. A. Kliore, in (5), p. 265.
18. M. I. Verigin *et al.*, *J. Geophys. Res.* **96**, 19307 (1991).
19. L. H. Brace, R. F. Theis, W. R. Hoegy, *Planet. Space Sci.* **30**, 29 (1982).
20. M. H. G. Zhang *et al.*, *J. Geophys. Res.* **95**, 17095 (1990).
21. J. A. Van Allen, L. A. Frank, S. M. Krimigis, H. K. Hills, *Science* **149**, 1228, (1965); J. J. O'Gallagher and J. A. Simpson, *ibid.*, p. 1233.
22. E. J. Smith, L. Davis Jr., P. J. Coleman Jr., D. E. Jones, *ibid.*, p. 1241.
23. S. S. Dolginov, *Geophys. Res. Lett.* **5**, 93 (1978); *ibid.*, p. 89; W. I. Axford, *Planet. Space Sci.* **39**, 167 (1991); D. Möhlmann *et al.*, *ibid.*, p. 83; D. S. Intrilligator and E. J. Smith, *J. Geophys. Res.* **84**, 8427 (1979); W. B. Hanson and C. P. Mantas, *ibid.* **93**, 7538 (1988).
24. C. T. Russell *et al.*, *Planet. Space Sci.* **43**, 875 (1995); C. T. Russell, *Geophys. Res. Lett.* **5**, 85 (1978); K. Schwingschuh *et al.*, *Adv. Space Res.* **12**, 213 (1992).
25. J. E. P. Connerney, *J. Geophys. Res.* **98**, 18659 (1993); N. F. Ness, *Philos. Trans. R. Soc. London Ser. A* **349**, 249 (1994); C. T. Russell, *J. Geophys. Res.* **98**, 18681 (1993).
26. G. Schubert *et al.*, in *Mars*, H. H. Kieffer *et al.*, Eds. (Univ. of Arizona Press, Tucson, 1992), pp. 147-183; W. M. Folkner, C. F. Yoder, D. N. Yuan, E. M. Standish, R. A. Preston, *Science* **278**, 1749 (1997).
27. L. L. Hood and K. Hartdegen, *Geophys. Res. Lett.* **24**, 727 (1997).
28. D. W. Collinson, *Meteorites Planet. Sci.* **32**, 803 (1997); S. M. Cisowski, *Geochim. Cosmochim. Acta* **50**, 1043 (1986).
29. R. D. Warner and P. J. Wasilewski, *J. Geophys. Res.* **102**, 20225 (1997).
30. R. A. Langel *et al.*, *Geophys. Res. Lett.* **9**, 269 (1982).
31. S. A. Curtis and N. F. Ness, *ibid.* **15**, 737 (1988). As suggested by a referee, a global field composed of the accumulated effect of a large number of anomalies could also prove to be important.
32. We thank the Mars Global Surveyor engineering and project personnel at Goddard Space Flight Center, Jet Propulsion Laboratory, Lockheed Martin Astronautics, and Spectrolab Incorporated for their support and the magnetic cleanliness of the spacecraft and solar panels. The contributions of J. Scheifele, E. Worthy, R. Berman, P. Panetta, J. Houser, M. Kirsch, F. Hunsaker, D. Chomay, M. Powell, R. Sterling, and J. Rouzaud to the development of the experiment and data processing system are gratefully acknowledged.

27 January 1998; accepted 13 February 1998